CHEMISTRY OF MATERIALS

ARTICLE

pubs.acs.org/cm

Alkali-ion Conduction Paths in $LiFeSO_4F$ and $NaFeSO_4F$ Tavorite-Type Cathode Materials

Rajesh Tripathi,[†] Grahame R. Gardiner,[‡] M. Saiful Islam,[*,‡] and Linda F. Nazar[*,†]

[†]Department of Chemistry, University of Waterloo, Waterloo, Ontario, Canada N2L 3G1

[‡]Department of Chemistry, University of Bath, Bath, United Kingdom BA2 7AY

ABSTRACT: A new family of fluorosulfates has attracted considerable attention as alternative positive electrode materials for rechargeable lithium batteries. However, an atomic-scale understanding of the ion conduction paths in these systems is still lacking, and this is important for developing strategies for optimization of the electrochemical properties. Here, the alkali-ion transport behavior of both $LiFeSO_4F$ and $NaFeSO_4F$ are investigated by atomistic modeling methods. Activation energies for numerous ion migration paths through the complex structures are calculated. The results indicate that $LiFeSO_4F$ is effectively a three-dimensional (3D) lithium-ion conductor with an activation energy of ~0.4 eV for long-range diffusion, which involve a combination of zigzag paths through [100], [010], and [111] tunnels in the open tavorite lattice. In contrast, for the related $NaFeSO_4F$, only one direction ([101]) is found to have a relatively low activation energy (0.6 eV). This leads to a diffusion coefficient that is more than 6 orders of magnitude lower than any other direction, suggesting that $NaFeSO_4F$ is a one-dimensional (1D) Na-ion conductor.

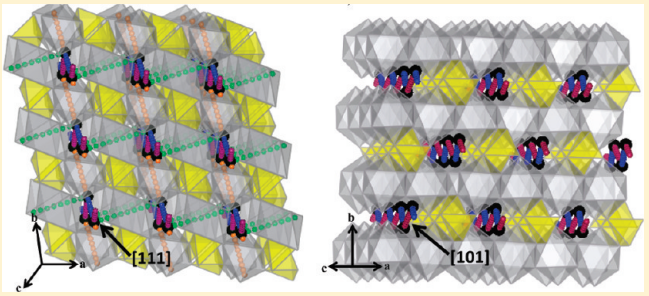

KEYWORDS: Li-ion battery, lithium iron fluorosulfate, sodium iron fluorosulfate, atomistic modeling, ion transport, lithium ion conductor, sodium ion conductor

INTRODUCTION

Over the last two decades, energy storage devices have experienced increased demand for higher energy density and superior power rates, leading to intensive research for new electrode materials. Li-ion batteries using layered oxide materials ($LiCoO_2$) were first commercialized in 1990, but its expense and safety issues have since led to a plethora of significant developments.[1] Among these, Padhi et al. proposed polyanionic transition metal phosphates ($LiFePO_4$) as an alternative in 1997, which adopt an olivine structure.[2] One-dimensional (1D) tunnels constructed from FeO_6 octahedra and PO_4 tetrahedra house the Li ions in this framework. However, the structure provides only one low activation energy pathway for Li ion migration along the 1D tunnels, and the conduction of electrons and ions is highly correlated.[3] These problems have been partially addressed through the use of conductive coatings and nanosizing the $LiFePO_4$ particles;[4,5] however, the inherent limitations of the structure remain an issue. The mystery of why the olivine lattice can exhibit such high rates, despite these factors, is still under debate.[6]

Recently, another polyanionic family of materials having fluorine as a network modifier in the structure framework has been reported as an excellent alternative.[7] Fluorophosphates as electrode materials were reported first by Barker et al.,[8] followed by detailed reports of their viability as better cathode materials by other groups.[9,10] Alkali-metal fluorophosphates form a large isostructural family of the chemical formula $AMPO_4F$, where A is an alkali metal and M is a transition metal. These structures are often named after their corresponding mineral member found abundantly in the Earth's crust, either as hydroxides or as fluorides. Most important are montebrasite ($LiAlPO_4OH$),[11] amblygonite ($LiAlPO_4F$),[12] and tavorite ($LiFePO_4OH$),[13] which are all essentially isostructural. The material $LiFePO_4F$, which crystallizes in this framework, has been shown to be an excellent ionic conductor and a reversible host for the Li^+ ion.[8] It exhibits a theoretical capacity of 145 mAh/g at 3 V (redox couple: Fe^{2+}/Fe^{3+}), which is lower than that of $LiFePO_4$ (3.4 V) analog, because of the difference in connectivity of the octahedral and tetrahedral moieties.

It has been shown previously that the open circuit voltage (OCV) of a material can be increased by tuning the covalency of the bonds in the polyanion.[14] In particular, replacing the PO_4^{3-} moiety by SO_4^{2-} in a polyanionic $LiMXO_4$ compound increases the OCV by ~0.6−0.8 V.[14] Taking a cue from such examples, successful attempts were made to improve the low OCV in tavorite materials. $LiFeSO_4F$ has been recently demonstrated to be an excellent cathode material.[15] It exhibits an OCV of 3.6 V and a theoretical capacity of 151 mAh/g. By comparison to $LiFePO_4$, the slightly lower capacity is compensated by the increased OCV and higher ionic conductivity of the material.[15] The energy density is thus only 5% lower, and higher power characteristics are potentially possible with nanostructured materials. Like $LiFePO_4$, $LiFeSO_4F$ can also be synthesized using abundantly available inorganic precursors in an inexpensive organic medium at low temperatures.[16] Possibly due to

Received: March 7, 2011
Revised: March 10, 2011
Published: March 30, 2011

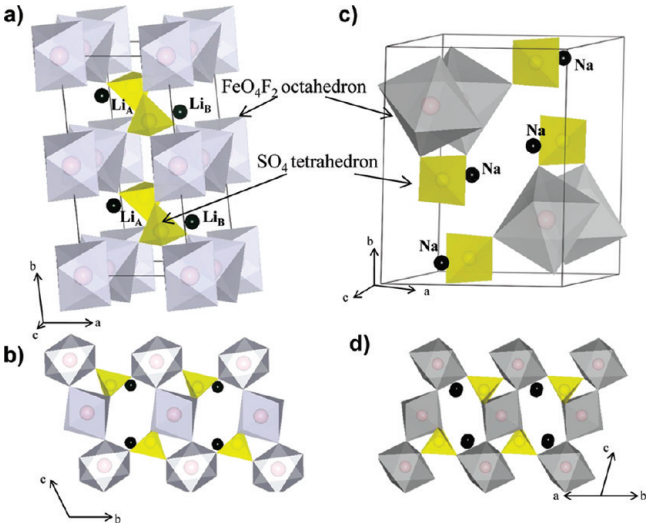

Figure 1. Depiction of the unit cells: (a) $LiFeSO_4F$ unit cell, modeled in a $P\bar{1}$ supercell with alternate occupation of two Li sites, where Li_A and Li_B represent the alternate full occupancy of the Li_1 and Li_2 sites, respectively; (b) a view into the tunnel along the [100] direction and position of Li ions inside (a similar geometry also exists for the tunnel along the [010] direction); (c) $NaFeSO_4F$ unit cell, modeled in the same unit cell as experimentally obtained ($P2_1/c$); and (d) a view into the tunnel along the [110] direction and position of Na ions inside (a similar geometry also exists for the tunnel along the [$\bar{1}$10] direction).

the presence of structural tunnels, the ionic conductivity of the material has been found to be better than its phosphate olivine analog, such as $LiFePO_4$. Nonetheless, apart from basic conductivity studies, there has been little attempt so far to understand the atomistic migration pathways or activation energies that govern the Li ion conduction within the structure.

Equally important is to examine Na-ion mobility in tavorite-type $NaFeSO_4F$.[16,17] Intermediate-scale Li-based batteries are the clear choice to fill the increasing demand to power plug-in hybrid vehicles and electric vehicles. These demands may put strain on the resources of lithium and, hence, on its cost effectiveness.[10] Moreover, a massive increase in demand for large-scale rechargeable batteries is predicted in the immediate future in the energy sector. Sodium, on the other hand, is an abundantly available resource. Thus Na-based batteries, where Na^+ ions replace Li^+ as the charge carrier, have been proposed as a viable alternative for very large-scale storage devices that could couple with renewable energy sources for load-leveling the electric grid. Demonstration of fairly effective cathode and anode materials that can reversibly insert/deinsert Na^+ has, in recent years, led to a surge in the search of other crystalline systems with better Na^+ insertion rate and capacity.[10] Recent successes include tavorite-type $NaVPO_4F$, and layered Na_2FePO_4F.[10,18] The fluorosulfate $NaFeSO_4F$ also crystallizes in a tavorite-type structure, albeit with a slightly different symmetry than that which is commonly observed. However, initial attempts to extract Na^+ ion from this structure have given very disappointing results that are puzzling, given the presence of open ion transport channels and reportedly good ionic conductivity.[17]

To fully understand the local structural and transport features influencing the electrochemical behavior of the $AFeSO_4F$ (A = Li or Na) materials, it is clear that fundamental knowledge of their underlying defect and transport properties is needed on the atomic scale. Atomistic modeling techniques provide a powerful means of investigating these key solid-state issues, but have not been applied to these fluorosulfates. The present work extends our recent simulation studies of $LiFePO_4$[3] and Li_2MSiO_4 (M = Fe, Mn)[19] with a comprehensive study on the energetics of intrinsic defects and alkali-ion migration in the tavorite-type $LiFeSO_4F$ and $NaFeSO_4F$ cathode materials.

EXPERIMENTAL SECTION

This study uses well-established modeling techniques, which are detailed elsewhere;[20] hence, only a general description will be given here. Interactions between ions in the fluorosulfate structures consist of a long-range Coulombic term and a short-range component representing electron−electron repulsion and van der Waals interactions. The short-range interactions were modeled using the two-body Buckingham potential.[20] An additional three-body term was used for the SO_4^{2-} units to account for the angle-dependent nature of O−S−O bonds, as previously used for other sulfates[23] and phosphates.[3] The well-known shell model[21] was employed to account for the polarizability effects of charged defects on the electronic charge clouds. The Fe−O and Li−O interatomic potentials were taken from the recent study[3] on $LiFePO_4$. The Na−O, S−O, O−F, Fe−F, and A-F (A = Li, Na) interactions were obtained by refining parameters from previous studies on fluorides and oxyfluorides.[22] For the sulfate component, the interatomic potential model successfully formulated to simulate M_2SO_4 (M = Na, K, Rb, and Cs) and XSO_4 (X = Sr, Ca, Ba)[23] was used. A Morse potential was used to describe intramolecular bond-stretching interactions between S and O ions in the sulfate group.

As argued previously, employing these interatomic potential methods is assessed primarily by its ability to reproduce observed crystal properties. Indeed, they are found to work well, even for compounds where there is undoubtedly a degree of covalency, such as aluminophosphates and silicates.[19,24]

The lattice relaxation about defects (such as Li vacancies) and migrating ions was calculated by an implementation of the Mott−Littleton scheme incorporated in the GULP code.[25] This method partitions a crystal lattice into two regions, where ions in the inner region immediately surrounding the defect (on the order of >700 ions) are relaxed explicitly. Relaxations of such a large number of ions are important for charge defects that introduce long-range electrostatic perturbations and are not easily treated by electronic structure methods. The outer region extends to infinity, with the outer lattice relaxations treated by quasi-continuum methods.

These techniques have been used successfully on a wide-range of inorganic solids, including recent work on ion transport in the cathode material[3] $LiFePO_4$ and the fuel cell electrolyte $LaBaGaO_4$.[26]

RESULTS AND DISCUSSION

Structural Modeling. The structure of $LiFeSO_4F$ belongs to the tavorite family of mineral structures, crystallizing in the triclinic $P\bar{1}$ space group.[15,16] The structure encompasses chains of alternately oriented corner-sharing FeO_4F_2 octahedra that run along the *c*-axis and share fluorine located on opposite vertices. Each of the four oxygen atoms in the polyhedron is also bonded to a sulfur atom, forming Fe−O−S−O−Fe chains that cross-link the structure (see Figure 1a). The separation between the FeO_4F_2 octahedral chains introduced by the corner-sharing SO_4 tetrahedra results in three primary open tunnels along the [100], [010], and [101] directions in the structure that house the Li ions. In $NaFeSO_4F$, the connectivity between the atoms is essentially the same, as can be seen in the structure illustrated in Figure 1d. However, the lattice adopts a higher symmetry space group ($P2_1/c$), compared to that of $LiFeSO_4F$ ($P\bar{1}$);[16] thus, there are subtle differences. Most importantly, the

dx.doi.org/10.1021/cm200683n |*Chem. Mater.* 2011, 23, 2278–2284

Table 1. Calculated and Experimental Structural Parameters for $AFeSO_4F$ (A = Li, Na)

	$LiFeSO_4F$			$NaFeSO_4F$		
lattice parameter	calc.	exp.	Δ	calc.	exp.	Δ
a (Å)	5.146	5.175	−0.029	6.648	6.673	−0.025
b (Å)	10.920	10.983	−0.063	8.676	8.699	−0.022
c (Å)	7.279	7.221	0.058	7.252	7.187	0.065
α (deg)	106.286	106.506	−0.220	90.000	90.000	0.000
β (deg)	107.272	107.177	0.095	111.839	113.524	−1.684
γ (deg)	96.121	97.866	−1.745	90.00	90.00	0.00

corresponding crystallographic directions between the two structures are different. They can be correlated by noting that the primary tunnels along the [100], [010], and [101] directions in $LiFeSO_4F$ correspond to the [110], [$\bar{1}$10], and [101] directions in $NaFeSO_4F$.

The starting structural parameters of the current simulation study were the observed crystal structure, in which the $LiFeSO_4F$ structure has been refined experimentally with two half-occupied Li sites.[16] This was modeled in a $P\bar{1}$ supercell with alternate occupation of these two sites, where Li_A and Li_B represent the alternate full occupancy of the Li1 and Li2 sites, respectively (see Figure 1a).

The potential parameters used in this study (discussed in the Experimental Section) were used to simulate optimized structures, with a direct comparison of experimental and calculated structures reported in Table 1. The calculated unit-cell parameters *a*, *b*, and *c* deviate from the experimental values by, at most, 0.07 Å (much less in most cases). The successful reproduction of the complex tavorite crystal structures provides additional support that the potential models can be used reliably in the defect and migration calculations.

Intrinsic Defects. As noted, insight into the defect properties of cathode materials is crucial to the full understanding of their electrochemical behavior. Isolated defect (vacancy and interstitial) energies were calculated for both $LiFeSO_4F$ and $NaFeSO_4F$, which were combined to determine the formation energies for Frenkel- and Schottky-type intrinsic defects. The following equations represent the reactions involving these defects (using Kröger−Vink notation and where A = Li or Na):

$$\text{A Frenkel}: \quad A_A^{\times} \rightarrow V_A^{'} + A_i^{\bullet} \tag{3}$$

$$\text{Fe Frenkel}: \quad Fe_{Fe}^{\times} \rightarrow V_{Fe}^{''} + Fe_i^{\bullet\bullet} \tag{4}$$

$$\text{F Frenkel}: \quad F_F^{\times} \rightarrow V_F^{\bullet} + F_i^{'} \tag{5}$$

$$\text{AF Schottky-type}: \quad A_A^{\times} + F_F^{\times} \rightarrow V_A^{'} + V_F^{\bullet} + AF \tag{6}$$

$$\text{FeF}_2\text{ Schottky-type}: \quad Fe_{Fe}^{\times} + F_F^{\times} \rightarrow V_{Fe}^{''} + 2V_F^{\bullet} + FeF_2 \tag{7}$$

We also examined the A/Fe "anti-site" pair defect involving the interchange of an A^+ ion with an Fe^{2+} ion, which is worth investigating, since Li/Fe "cation exchange" effects have been a significant topic of discussion for $LiFePO_4$.[3] This process can be described by the following equation:

$$\text{Anti-site}: \quad A_A^{\times} + Fe_{Fe}^{\times} \rightarrow A_{Fe}^{'} + Fe_A^{\bullet} \tag{8}$$

Examination of the resulting defect energies listed in Table 2 reveal two main predictions. First, the formation of all Frenkel and Schottky defects is unfavorable in both $AFeSO_4F$ structures. Interestingly, the results suggest that fluoride vacancies and fluoride interstitials are unlikely to exist in the pure (undoped) materials. Second, the antisite energies are also relatively high, which indicates that there would be no significant concentration of Fe on A sites at operating temperatures in these tavorite-type fluorosulfates. This is in contrast with the $LiFePO_4$ material, which exhibits cation exchange behavior, particularly Fe on Li sites. Therefore, these results suggest that conduction "blocking" effects involving Fe on Li or Na sites are much less likely in the $AFeSO_4F$ cathode materials.

Table 2. Energies of Intrinsic Defect Processes in $AFeSO_4F$ (A = Li, Na)

		Energy (eV)	
disorder type	equation	$LiFeSO_4F$	$NaFeSO_4F$
A Frenkel	(3)	3.79	2.99
Fe Frenkel	(4)	7.60	10.09
F Frenkel	(5)	4.84	3.10
AF Schottky-type	(6)	4.22	4.10
FeF_2 Schottky-type	(7)	8.38	8.23
A/M antisite	(8)	2.50	2.40

Li-Ion Migration. Using atomistic simulation techniques, it is possible to examine various possible transport paths that are responsible for Li^+ (or Na^+) conduction, which are often difficult to probe on the atomic scale by experiment alone. Energy profiles for conduction paths via the conventional hopping model can be derived by calculating the energy of the migrating ion in the adjacent Li sites. Relaxation of the surrounding lattice (>700 ions) is treated explicitly by these defect modeling methods. The position of highest potential energy along the migration path corresponds to the migration activation energy.

In the $LiFeSO_4F$ unit cell, there are two Li sites (labeled Li_A and Li_B in Figure 1a). These occupy two diametrically disposed positions in the tunnels that run along either the [100] or [010] directions, as shown in the long-range view of the structure (Figure 1b). From this, we have identified the main migration paths between adjacent Li sites. There are three possible Li−Li jump distances along the [100] direction and three Li−Li jump distances along the [010] direction, as shown in Figure 2a. These jumps (L1−L6) represent all the possible migration paths between adjacent Li sites.

The calculated activation energies for Li-ion migration in $LiFeSO_4F$ are included in Figure 2a (and are listed in Table 3a), revealing three main points. First, the lowest migration energies are 0.36−0.46 eV for jumps involving paths L3−L6. Such relatively low values suggest high Li mobility in the $LiFeSO_4F$ material, which is important for good electrochemical behavior.

Second, the results indicate that the favorable Li migration paths are a combination of two diagonal jumps. These diagonal or zigzag jumps form continuous pathways through the structure and allow long-range diffusion along the tunnels in the [100], [010], and [111] directions, with the lowest-energy path being along the [111] direction. The three-dimensional (3D) view of the structure (Figure 4a) reveals that four unique jumps (L3−L6) are possible for each Li ion (see Figures 2a and 2b), which leads to continuous interconnecting paths and effective 3D transport of Li ions. We should note that L1 and L2 are hops

dx.doi.org/10.1021/cm200683n |*Chem. Mater.* 2011, 23, 2278–2284

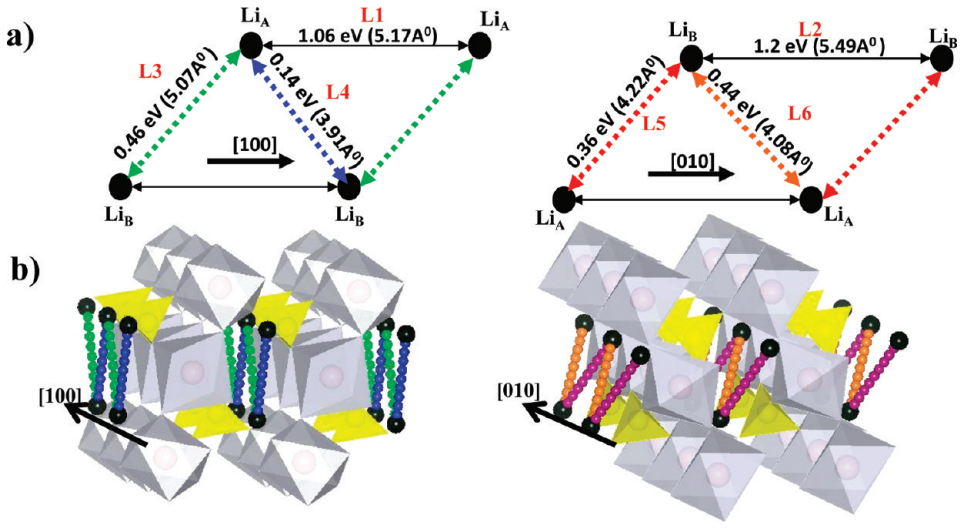

Figure 2. (a) Schematic illustrating the various Li distances in tavorite $LiFeSO_4F$ along the primary tunnels [100] and [010]; the preferable Li-ion hopping paths are shown as dashed lines, where each color belongs to a unique hop with a distinct activation energy. (b) Corresponding long-range transport within the lattice; the same color code as that described in panel a is followed.

Table 3. Calculated Activation Energies for the Most Favorable Paths of Alkali-Ion Migration: (a) Li-Ion Migration in $LiFeSO_4F$ (b) Na-Ion Migration in $NaFeSO_4F$ (Paths Are Shown in Figures 2 and 3)

(a) Li-Ion Migration in $LiFeSO_4F$

net diffusion direction	jumps involved	activation energy (eV)
[100]	L3 + L4	0.46
[010]	L5 + L6	0.44
[001]	L3 + L6	0.46
[101]	L4 + L6	0.44
[011]	L3 + L5	0.46
[111]	L4 + L5	0.36

(b) Na-Ion Migration in $NaFeSO_4F$

net diffusion direction	jumps involved	activation energy (eV)
[100]	N3 + N4 + N5	0.91
[010]	N3 + N4 or N3 + N5	0.91
[001]	N5	0.91
[110]	N3 + N4 + N5	0.91
[$\bar{1}$10]	N3 + N4 + N5	0.91
[101]	N4 + N5	0.60

between symmetry-equivalent sites (i.e., Li_A-Li_A), along the [100] and [010] directions, respectively, and are found to have high and unfavorable activation energies (>1.0 eV); this is probably due to the migrating Li ion coming into close proximity to the FeO_4F_2 octahedra.

Finally, although direct comparison with Li-ion conductivity data is not straightforward, our calculated values of ~0.4 eV is consistent with experimental activation energies for Li diffusion in other related cathodes or LISICON-type materials.[27]

The diffusion coefficient of any ion hop, according to dilute diffusion theory, can be estimated using[28]

$$D = g\Gamma a^2$$

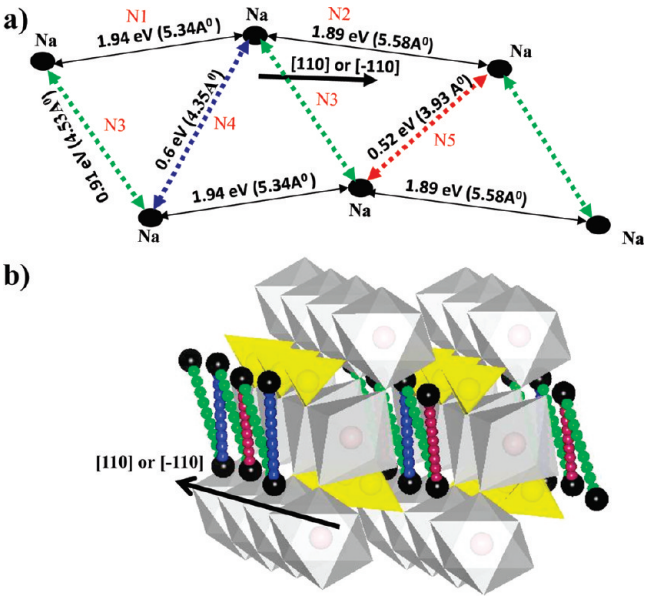

Figure 3. (a) Schematic showing the various Na−Na distances in $NaFeSO_4F$ along the primary tunnels [110] or [$\bar{1}$10]; the preferred Na-ion hopping paths are depicted in color, where each color belongs to a unique hopping activation energy. (b) Corresponding long-range transport within the lattice; the same color code as that described in panel a is followed.

where D is the chemical diffusion coefficient, g the geometric factor, and a the hop distance. Γ is the hopping frequency, as defined according to transition-state theory:[29]

$$\Gamma \approx \nu^* \exp\left(\frac{-E_a}{kT}\right)$$

In this case, ν is the attempt frequency and E_a is the migration activation energy. Thus, the activation energy gives a direct estimate for the diffusion coefficient over a specific hop distance. For our calculations, g is assumed to be equal to 1 and we use the typical value[29] for ν of 10^{13} s^{-1}.

dx.doi.org/10.1021/cm200683n |Chem. Mater. 2011, 23, 2278–2284

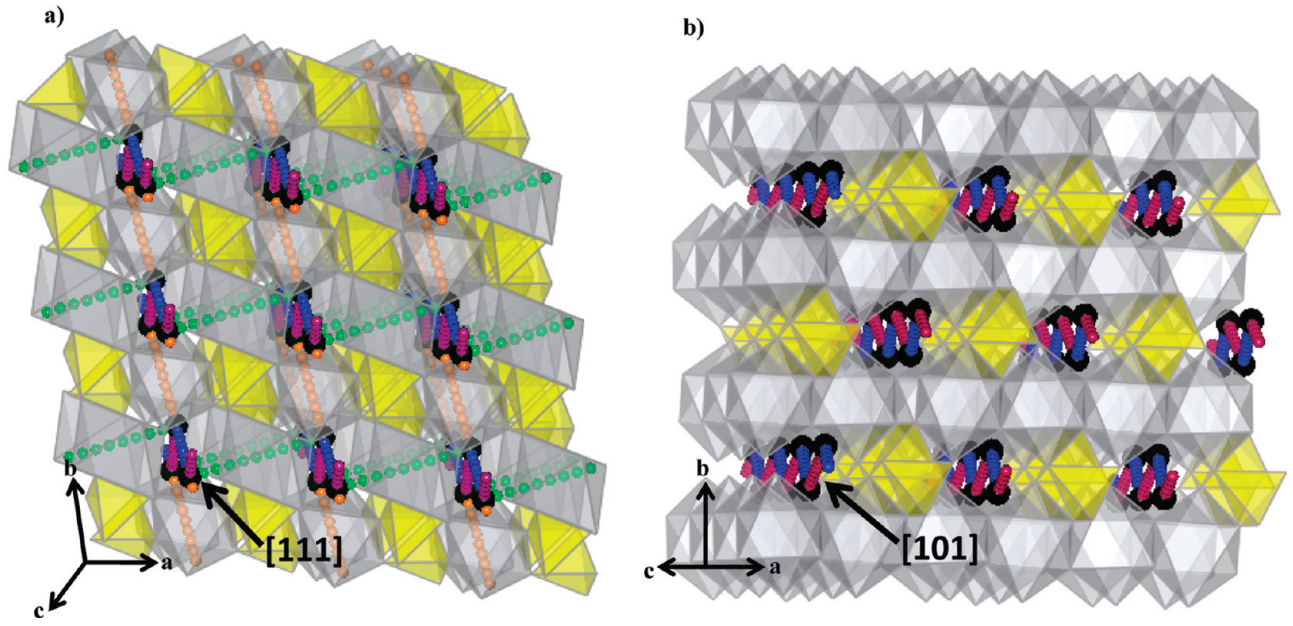

Figure 4. Full view of the structures and ion conduction pathways: (a) 3D Li-ion conduction in $LiFeSO_4F$ and (b) 1D Na-ion conduction in $NaFeSO_4F$. The same color code as that described in Figures 2 and 3 has been used.

Dilute diffusion theory can be assumed to be reasonably valid for fluorosulfate materials, even during the (de)lithiation process. According to previous studies,[15,16] (de)lithiation occurs via a two-phase process over most of the compositional range. In this case, the new phase formed upon (de)lithiation remains almost stoichiometric in nature, thus giving a very dilute, and therefore noninteracting, concentration of the charge-carrying defects (Li^+ ions or vacancies). For the favorable activation energies in $LiFeSO_4F$, the diffusion coefficients are estimated to be in the range of $10^{-10} - 10^{-8}$ cm^2/s, which is consistent with values found for the conventional cathode $LiCoO_2$.

Depending upon synthesis conditions, experimental values of the activation energy for Li ion mobility in fluorosulfate tavorites measured by impedance spectroscopy are reported to be in the range 0.77−0.99 eV for $LiFeSO_4F$[15,30] and 0.94 eV for $LiMgSO_4F$.[31] An estimated diffusion coefficient using such values of the activation energy would be of the order of $\sim 10^{-19}$ cm^2/s, implying extremely limited ion mobility. These values are in contrast to the excellent electrochemical and ion-conducting behavior (respectively) exhibited by these two materials. $LiFeSO_4F$ is known to have low thermal stability; therefore, as noted earlier,[15] the inability to hot-press the material leads to poor particle−particle contact and could lead to high experimental activation energy values. A minimum value of 0.3 eV for $LiFeSO_4F$ has been calculated along an unspecified direction using density functional theory (DFT) methods.[32] The discrepancy between the calculated and experimentally measured activation energies have been rationalized[32] by including Li vacancy formation energy in stoichiometric $LiFeSO_4F$. However, this is unlikely, because the thermodynamic minimum, which is guided by the entropy of the system, always exists at a certain nonzero point-defect concentration. Thus, such systems will always have a finite concentration of Li vacancies.

Na-Ion Migration. $NaFeSO_4F$ crystallizes in a different space group ($P2_1/c$) to $LiFeSO_4F$ ($P\bar{1}$) with only one Na^+ ion site in the unit cell (Figure 1b). Hence, the two intersecting tunnels that are inequivalent in $LiFeSO_4F$ (along the [100] and [010] directions), become equivalent in $NaFeSO_4F$ (i.e., along the [110] and [$\bar{1}$10] directions). Therefore, only one schematic is shown in Figure 3a. As with $LiFeSO_4F$, we have identified the main migration paths in $NaFeSO_4F$ between adjacent Na sites. The calculated activation energies for Na-ion migration in $NaFeSO_4F$ are included in Figure 3a (and are listed in Table 3b), indicating two key results.

First, the lowest migration energy is 0.6 eV for jumps involving paths N4 and N5, with other paths (N3−N5) that involve short Na−Na distances (<4.5 Å) having activation energies of ∼0.9 eV. Hence, the Na migration energies in $NaFeSO_4F$ are higher than that for Li migration in $LiFeSO_4F$, which suggests lower Na mobility. However, we note that the tunnel-structured material $Na_4TiP_2O_9$ has been reported to be a Na-ion conductor with an activation energy as high as 1 eV, based on single-crystal experiments.[33]

Second, the favorable Na migration paths are also a combination of diagonal or zigzag jumps forming continuous diffusion pathways through the structure. However, diffusion coefficients estimated for these migration paths of 0.6 and 0.9 eV are 1.2×10^{-12} and 8×10^{-18} cm^2/s, respectively. This large difference in magnitude indicates that Na^+-ion diffusion in $NaFeSO_4F$ is effectively one-dimensional. The 3D view of the structure (Figure 4b) reveals that the lowest-energy path (0.6 eV) leads to continuous interconnecting paths, but only through the [101] tunnel and effective 1D Na^+ transport. As in $LiFeSO_4F$, the highest-energy migration jump (1.9 eV) involving N1 and N2 is close to the FeO_4F_2 octahedra, which is probably due to stronger steric interactions with the larger Na ion.

Overall, these simulations suggest that the ionic conductivity of $NaFeSO_4F$ should be lower than $LiFeSO_4F$. It has been noted earlier[16] that split site occupancy of Li ions, as opposed to a fixed Na-ion site, may indicate higher Li-ion mobility in the structure, and this is also confirmed by comparing bond sums (0.99 in $LiFeSO_4F$ vs 1.16 in $NaFeSO_4F$). However, direct comparison with electrochemical behavior is not straightforward. Indeed, electrochemical (de)insertion in any electrode is not solely dependent on the ionic conductivity.[34] The electrochemical

properties of $NaFeSO_4F$ may not be solely driven by low ion conductivity. These may be nested in the two-phase driven (de)intercalation process (with a 14.5% volume difference[16] in the end-member phases), which adds a substantial additional phase-boundary migration energy term. These issues warrant further investigation, as well as detailed studies on the electronic structure using DFT-based methods.

CONCLUSIONS

This investigation of tavorite-type fluorosulfates has provided atomic-scale insights into the intrinsic defect chemistry and alkali-ion conduction paths, which are relevant to their electrochemical behavior as new lithium battery cathodes. The main results can be summarized as follows:

(1) Our simulations show good reproduction of the observed structures of both $LiFeSO_4F$ and $NaFeSO_4F$. The defect calculations indicate that the formation of all Frenkel and Schottky intrinsic defects is unfavorable. The Li/Fe and Na/Fe anti-site energies also suggest that there would be no significant intrinsic concentration of Fe on Li or Na sites at operating temperatures in these fluorosulfates. This is in contrast with the $LiFePO_4$ cathode material, which has a small amount of Fe on Li sites.

(2) Investigation of the transport paths in $LiFeSO_4F$ indicates relatively low migration energies (~0.4 eV), suggesting high Li mobility, which is important for good rate capability and capacity retention. The Li migration paths are a combination of diagonal jumps that form continuous diffusion pathways in the open tavorite structure. Li^+ transport is found to be effectively three-dimensional in $LiFeSO_4F$, with diffusion along tunnels in the [100], [010], and [111] directions, with the lowest energy path being along the [111] direction.

(3) Na-ion transport in monoclinic $NaFeSO_4F$ is also mediated by a combination of zigzag jumps, but with higher activation energies (~0.9 eV) than that for Li-ion migration in $LiFeSO_4F$. The estimated diffusion coefficient for the most favorable migration path through the [101] tunnel is at least 6 orders of magnitude higher than that in any other direction, suggesting that $NaFeSO_4F$ is, effectively, a one-dimensional Na-ion conductor.

Such differences in intrinsic alkali-ion mobility would influence the ability to extract Li and Na from the $LiFeSO_4F$ and $NaFeSO_4F$ structures and, hence, lead to contrasting capacity retention and rate capability as rechargeable electrodes. These transport properties, coupled with the two-phase behavior of (de)intercalation of alkali ions and a large volume difference between end members, helps to rationalize the difference in the observed electrochemical behavior of the Li and Na fluorosulfates.

AUTHOR INFORMATION

Corresponding Author

*E-mail addresses: lfnazar@uwaterloo.ca (L.F.N.), m.s.islam@bath.ac.uk (M.S.I.).

ACKNOWLEDGMENT

L.F.N. gratefully acknowledges NSERC through funding from its Discovery, Canada Research Chair and Collaborative Research (with GM) programs. M.S.I. acknowledges funding from the EPSRC Supergen.

REFERENCES

(1) Ellis, B. L.; Lee, K. T.; Nazar, L. F. *Chem. Mater.* **2010**, *22*, 691–714.
(2) Padhi, A. K.; Nanjundaswamy, K. S.; Goodenough, J. B. *J. Electrochem. Soc.* **1997**, *144*, 1188–1194.
(3) (a) Islam, M. S.; Driscoll, D. J.; Fisher, C. A. J.; Slater, P. R. *Chem. Mater.* **2005**, *17*, 5085–5092.(b) Morgan, D.; Van der Ven, A.; Ceder, G. *Electrochem. Solid State Lett. 2004*, *7*, A30−A32.
(4) Gibbot, P.; Cabanas, M. C.; Laffont, L.; Levasseur, S.; Carlach, P.; Hamelet, S.; Tarascon, J. M.; Masquelier, C. *Nat. Mater.* **2008**, *7*, 741–747.
(5) Herle, P. S.; Ellis, B. L.; Coombs, N.; Nazar, L. F. *Nat. Mater.* **2004**, *3*, 147–152.
(6) (a) Tang, M.; Huang, H.-Y.; Meethong, N.; Kao, Y.-H.; Carter, W. C.; Chiang, Y.-M. *Chem. Mater.* **2009**, *21*, 1557–1571. (b) Zhou, F.; Maxisch, T.; Ceder, G. *Phys. Rev. Lett.* **2006**, *57*, 155074–155077.
(7) Yin, S. C.; Edwards, R.; Taylor, N.; Herle, P. S.; Nazar, L. F. *Chem. Mater.* **2006**, *18*, 1745–1752.
(8) Barker, J.; Saidi, M. Y.; Swoyer J. U.S. Patent 6,387,567, 2002.
(9) Ramesh, T. N.; Lee, K. T.; Ellis, B. L.; Nazar, L. F. *Electrochem. Solid State Lett.* **2010**, *13*, A43–A47.
(10) Ellis, B. L.; Makahnouk, W. R. M.; Makimura, Y.; Nazar, L. F. *Nat. Mater.* **2007**, *6*, 749–753.
(11) Baur, W. H. *Heidelb. Beitr. Mineral. Petrogr.* **1959**, *6*, 399–408.
(12) Simonov, V. I.; Belov, N. V. *Kristallografiya* **1958**, *3*, 429–430.
(13) Roberts, A. C.; Dunn, P. J.; Grice, J. D.; Newbury, D. E.; Dale, E.; Roberts, W. L. *Powder Diffr.* **1988**, *3*, 93–94.
(14) Padhi, A. K.; Nanjundaswamy, K. S.; Masquelier, C.; Goodenough, J. B. *J. Electrochem. Soc.* **1997**, *144*, 2581–2586.
(15) Recham, N.; Chotard, J. N.; Dupont, L.; Delacourt, C.; Walker, W.; Armand, M.; Tarascon, J.-M. *Nat. Mater.* **2010**, *9*, 68–74.
(16) Tripathi, R.; Ramesh, T. N.; Ellis, B. L.; Nazar, L. F. *Angew. Chem., Int. Ed.* **2010**, *49*, 8738–8742.
(17) Barpanda, P.; Chotard, J. N.; Recham, N.; Delacourt, C.; Ati, M; Dupont, L.; Armand, M.; Tarascon, J. M. *Inorg. Chem.* **2010**, *49*, 7401–7413.
(18) Barker, J.; Saidi, M. Y.; Swoyer, J. *J. Electrochem. Soc.* **2004**, *151*, A1670–A1677.
(19) Kuganathan, N.; Islam, M. S. *Chem. Mater.* **2009**, *21*, 5196–5202.
(20) Catlow, C. R. A. *Computer Modeling in Inorganic Crystallography*; Academic Press: San Diego, CA, 1997.
(21) Dick, B. G.; Overhauser, A. W. *Phys. Rev.* **1958**, *112*, 90–103.
(22) (a) Jackson, R. A.; Valerio, M. E. G.; Lima, J. F. *J. Phys.: Condens. Matter* **1996**, *8*, 10931–10937. (b) Islam, M. S.; D'Arco, S. *Chem. Commun.* **1996**, 2291–2292.
(23) (a) Allan, N. L.; Rohl, A. L.; Gay, D. H.; Catlow, C. R. A.; Davey, R. J.; Mackrodt, W. C. *Faraday Discuss.* **1993**, *95*, 273. (b) Redfern, S. E.; Parker, S. C. *J. Chem. Soc. Faraday Trans.* **1998**, *94*, 1947–1952. (c) Sastre, G.; Gale, J. D. *Chem. Mater.* **2005**, *17*, 730. (d) Gomez-Hortiguela, L; Cora, F; Catlow, C. R. A.; Perez-Pariente, J. *J. Am. Chem. Soc.* **2004**, *126*, 12097.
(24) Henson, N. J.; Hay, P. J.; Redondo, A. *J. Phys. Chem.* **2000**, *104*, 2423–2431.
(25) Gale, J. D.; Rohl, A. L. *Mol. Simul.* **2003**, *29*, 291–341.
(26) Kendrick, E.; Kendrick, J.; Knight, S. K.; Islam, M. S.; Slater, P. R. *Nat. Mater.* **2007**, *6*, 871–875.
(27) Sebastian, L.; Gopalakrishnan, J. *J. Mater. Chem.* **2003**, *13*, 433–441.
(28) Kutner, R. *Phys. Lett.* **1981**, *81*, 239–240.
(29) Van Der Ven, A.; Ceder, G. J. *Power Sources* **2001**, *97−98*, 529–531.
(30) Ati, M; Sougrati, T. M.; Recham, N.; Barpanda, P.; Leriche, J. B.; Courty, M.; Armand, M.; Jumas, J. C.; Tarascon, J. M. *J. Electrochem. Soc.* **2010**, *157*, A1007–A1015.

(31) Sebastian, L.; Gopalakrishnan, J.; Piffard, Y. *J. Mater. Chem.* **2002**, *12*, 374–377.
(32) Liu, Z.; Huang, X. *Solid State Ionics* **2010**, *181*, 1209–1213.
(33) Schitz, A. K. I. *Solid State Ionics* **1997**, *100*, 149–152.
(34) Ellis, B. L.; Perry, L. K.; Ryan, D. H.; Nazar, L. F. *J. Am. Chem. Soc.* **2006**, *128*, 11416–11422.